Probabilistic Seismic Performance Assessment of a Bridge-Foundation-Soil System

B.A. Bradley, M. Cubrinovski, R.P. Dhakal & G.A. MacRae

University of Canterbury, Christchurch, New Zealand.

2009 NZSEE Conference

ABSTRACT: This paper presents the probabilistic seismic performance assessment of an actual bridge-foundation-soil system, the Fitzgerald Avenue twin bridges. A two-dimensional plane strain finite element model of the longitudinal direction of the bridge-foundation-soil system is modelled using advanced soil and structural constitutive models. Ground motions are selected based on the seismic hazard deaggregation at the site, which is dominated by both fault and distributed seismicity. Based on rigorous examination of several deterministic analyses, engineering demand parameters (EDP's) are determined which capture the global and local demand and damage to the bridge and foundation, and multiple ground motions at various intensity levels are used to conduct seismic response analyses of the system.

It was found that the non-horizontal layering of the sedimentary soils has a pronounced effect on the seismic demand distribution to the bridge components, of which the north abutment piles and central pier are critical in the systems seismic performance.

1 INTRODUCTION

Methods for assessment of the seismic performance of soil-structure systems have evolved significantly in the past two decades. This evolution has involved further improvement of simplified design-oriented approaches, and also development of more robust, and complex, analysis procedures. In addition to the development in methods of analysis, attention has shifted from the implicit assessment of seismic performance via seismic response analysis, to an explicit consideration of seismic performance based on the consequences of seismic response and associated damage.

Consideration of the seismic response of soil-structure systems is complicated by the complexity of the ground motion excitation and the non-linear dynamic response of soil-structure systems. In addition to this complexity, the seismic response of soil-structure systems is burdened by a significant amount of uncertainty. Such uncertainty arises due to the uncertain nature of future ground motions which will occur at the site, as well as the lack of knowledge of the properties governing the response of the soil-structure system. In addition to the ground motion and seismic response uncertainties there are also uncertainties associated with the levels of damage to the structure and the corresponding consequences in terms of direct repair costs and loss of functionality and human injuries.

Recent efforts (e.g. Bradley, et al. 2008), predominantly following the Pacific Earthquake Engineering Research (PEER) Centre framework formula have focused on performance-based methodologies which allows the computation of seismic performance measures encompassing direct and indirect consequences associated with the seismic response of engineered facilities as well as addressing the significant aforementioned uncertainties in the seismic assessment problem.

The focus of this paper is the probabilistic seismic performance assessment of a two-span bridge structure supported on pile foundations which are founded in liquefiable soils. Firstly, the structure, site conditions, and computational model of the soil-pile-bridge system are discussed. An overview of the seismic response of the system for a single ground motion is discussed to elucidate the predominant deformation mechanisms of the system and to identify the engineering demand parameters (EDP's) to use in the probabilistic seismic demand assessment. Ground motions are

selected in accordance with the seismic hazard deaggregation for various intensity levels, and the results of the seismic response analyses are used to perform probabilistic seismic demand assessments of the system.

2 CASE STUDY: FITZGERALD AVENUE BRIDGES

2.1 *Details of the structure*

The Fitzgerald Avenue twin bridges are located near to the north-west of central Christchurch, New Zealand. Each of the two-span bridges is 30 m long, 12.1 m wide and 3.2 m high (Figure 1a). The 15 m bridge deck spans consist of 21 prestressed concrete I-girders and cast-in-place concrete slabs. The bridge superstructure is supported on two seat abutments and one central pier (Figure 1b). The abutments and pier are 2.5 m high and are the same width as the superstructure deck and are supported on pile group foundation consisting of 8 - 0.3 m diameter piles. All piles have continuous moment connections at the pile cap. At both abutments the bridge deck is seated on a 10 mm bearing pad as illustrated in Figure 1c.

Because of their location in the transportation network, the Fitzgerald Avenue bridges have been designated by the Christchurch City Council as a key lifeline for post-earthquake transportation. A recent assessment of the bridge structure recommended the installation of two additional driven piles at each of the abutments and central pier to a depth of 25 m. The two piles on each side of the central pier are 1.5 m in diameter, while those at the abutments are 1.2 m in diameter.

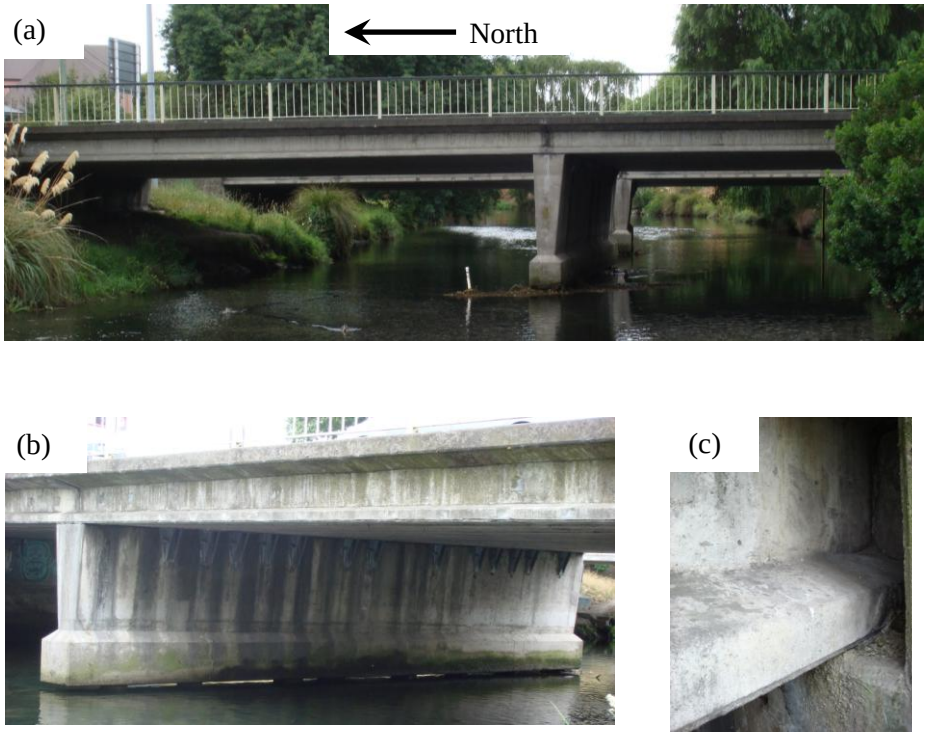

Figure 1: The Fitzgerald Avenue twin bridges: (a) elevation of the west bridge; (b) illustration of the central pier and pile cap; and (c) seating connection of bridge deck on abutments.

2.2 *Site conditions*

Previous site investigations conducted to confirm ground conditions and assess material strengths and liquefaction potential include: boreholes with standard penetrometer tests (SPT's); cone penetrometer tests (CPT's) with direct push Dual Tubes (DT's); and installation of piezometers. Based on these site investigations, the generic soil profile for the longitudinal axis of the bridge given in Figure 2 was developed. The soil profile consists of four distinct layers. The shallowest two horizontal layers have

thicknesses of 4.5 m and 6.5 m, and normalised SPT blowcounts of N_1 = 10 and N_1 = 15, respectively. Below these two layers, the profile deviates from a simple horizontal layering, with a weaker layer of 6.5 m depth and SPT blowcount of N_1 = 10 on the left hand side of the model. Below 17.5 m on the left hand side of the model, and up to 11m depth on the right hand side of the model is a significantly stiffer layer of N_1 = 30. Both the N_1 = 10 and N_1 = 15 layers are highly susceptible to liquefaction, while the N_1 = 30 base layer was deemed to be of a significantly lower liquefaction potential. Behind the abutments, gravel backfills extend at an angle of 30 degrees above horizontal to the surface.

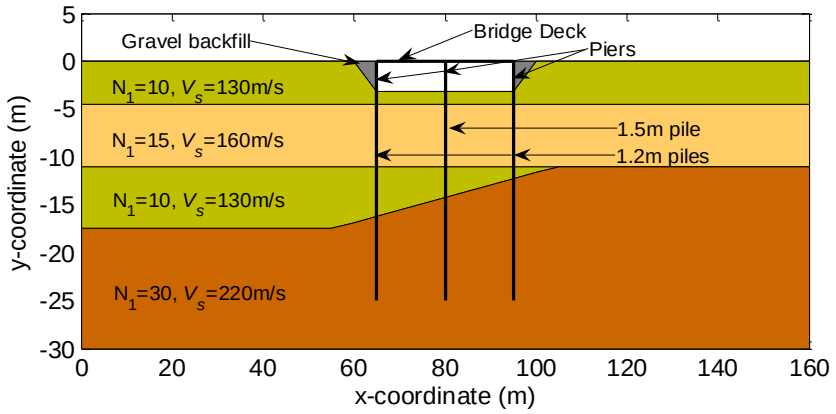

Figure 2: Schematic illustration of generic soil profile used in the computational model.

3 COMPUTATIONAL MODEL

A non-linear finite element plane-strain model of longitudinal direction of the bridge-foundation-soil system was constructed in the finite element program Diana-J (1987). While the seismic response of the bridge-pile-soil system is clearly a 3-dimensional problem, only the analyses of the longitudinal direction are discussed herein. Details of the effective stress analyses of the transverse direction of the bridge system are presented in Bowen and Cubrinovski (2008) and Cubrinovski and Bradley (2009). Because of their small aspect, it is likely that deformation in the transverse direction is critical for shear failure of the abutments and central pier.

Because of symmetry, the out-of-plane width of the longitudinal plane-strain model was taken to be half of the bridge width (6.05 m). That is, half of the bridge deck, abutments and piers were considered, as well as the same dimension for the soil thickness. Therefore, in the computational model, each abutment and pier is supported by a single 1.2 m and 1.5 m pile, respectively. The 0.3 m diameter piles which supported the structure before the installation of the 1.2 m and 1.5 m piles provide negligible contribution and were not considered in the computational model.

Because of the high liquefaction potential of the foundation soil, its dynamic response was considered to be a dominant feature affecting the response of the bridge-pile-soil system. The soil was modelled using the two-phase (soil-water) Stress-Density (S-D) constitutive model of Cubrinovski and Ishihara (1998). Further details on the computation of the constitutive model parameters used in the analysis is given in Bowen and Cubrinovski (2008) and Cubrinovski and Ishihara (1998), respectively.

The bridge abutments, central pier and pile foundations were modelled using displacement-based beam elements with three gauss points. At each gauss point, the moment-curvature response was parameterized by a hyperbolic curve, with the initial stiffness, EI, and peak moment, M_F, chosen to match the moment curvature relationship of the pile (See Bowen and Cubrinovski (2008) for details). The unloading/reloading path for the moment-curvature relationship is based on the Masing rule, and no strength degradation was considered due to limitations of the constitutive model. The bridge superstructure was modelled as linear elastic because of its significantly higher axial stiffness compared to the lateral stiffness of the abutments/piers and its higher flexural and shear strength.

A static analysis of the model was performed in order to determine the initial stress distribution in the model. In particular, a correct distribution of shear stresses near the abutments is critical for modelling

the tendency for lateral spreading of soil toward the river channel.

In addition to hysteretic damping occurring as a result of the inelastic constitutive models, Rayleigh damping was used to provide enhanced numerical stability with parameters $\alpha = 0$ and $\beta = 0.005$.

4 SEISMIC HAZARD AND GROUND MOTIONS

The seismic hazard due to earthquake-induced ground motion is determined using probabilistic seismic hazard analysis (PSHA). In order to obtain the seismic hazard curve it is first necessary to specify which ground motion intensity measure (IM) is to be used. In this study, *PGA* is used as the IM, both for its historical use and because it and spectral accelerations at various periods are the only IM's for which seismic hazard curves are publicly available for this location. Recent studies (Bradley, et al. 2008) have shown however that velocity-based IM's (e.g. peak ground velocity, *PGV*, and spectrum intensity, *SI*) are better IM's for such analyses of structures in liquefiable soils.

Figure 3a illustrates the ground motion hazard at the site of the bridge structure, while Figure 3b illustrates the hazard deaggregation used for ground motion selection. Ground motion selection in accordance with the seismic hazard deaggregation has been shown important (Shome and Cornell 1999), particularly for inefficient and insufficient IM's such as *PGA*. As noted in Stirling (2007) and evident in Figure 3b the seismic hazard is dominated by: (i) $M_W = 5.5\text{-}6.5$ earthquakes at short distances ($R = 15\text{-}30$ km), associated with background seismicity, and (ii) larger ($M_W = 7\text{-}7.5$) earthquakes on mapped faults ranging from $R = 25\text{-}50$ km.

Ground motions were selected for seismic response analyses at 9 different intensity levels as shown in Figure 3a. For each intensity level, ground motions were selected from the NGA database based on the M_w, R and ε deaggregation. A further limitation of an amplitude scale factor in the range, $SF = 0.6\text{-}1.6$, was used to help ensure that ground motions with the correct frequency content (i.e. spectral shape) were selected.

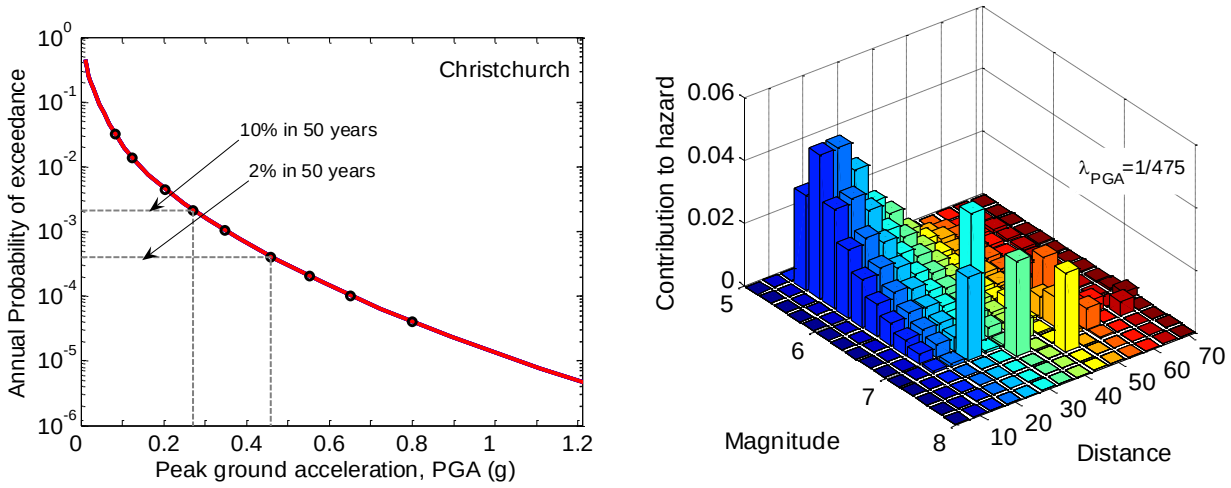

Figure 3: Details of the PGA seismic hazard for class C soil in Christchurch: (a) Seismic hazard curve; (b) Deaggregation of the hazard curve for λ_{PGA}=1/475; and (c) Ground motion target spectra for λ_{PGA}=1/475.

5 DETERMINISTIC PERFORMANCE ASSESSMENT

Before conducting the probabilistic seismic response analyses with multiple ground motions and at multiple intensity levels, it is necessary to first rigorously examine the computational model and its response to various levels of ground motion excitation. This is important for: (i) verification of the analysis algorithms, (ii) validation of the computational model with engineering judgment and observations, and (iii) to understand the predominant deformation mechanisms which control the response. The latter point, in particular, is necessary before conducting probabilistic effective stress analyses since the number of analyses means it is not feasible to examine each analysis in detail, with

various engineering demand parameter (EDP's) simply used to indicate the seismic response. Thus an understanding of the deformational mechanism is critical in the selection of appropriate EDP's, and below the seismic response of the computational model is illustrated for a single ground motion scaled to an intensity level with a 2% probability of exceedance in 50 years (i.e. 0.463g *PGA* from Figure 3a).

5.1.1 *Foundation soil response*

Figure 4 illustrates the development of excess pore pressures and eventual liquefaction in the soil surrounding the bridge. It can be seen that pore pressure ratios in the range $EPWPR$ = 0.2-0.5 first develop in the bottom N_1 = 10 layer on the left hand side of the model, and at the base of the N_1 = 15 layer on the right hand side of the model. The bottom N_1 = 10 layer has almost entirely liquefied by 6.0 seconds. As time progresses, pore water pressures continue to increase in the N_1 = 15 layer on the right hand side of the model, and the re-distribution of excess pore pressures causes liquefaction to spread to shallower depths (predominantly on the left hand side of the model).

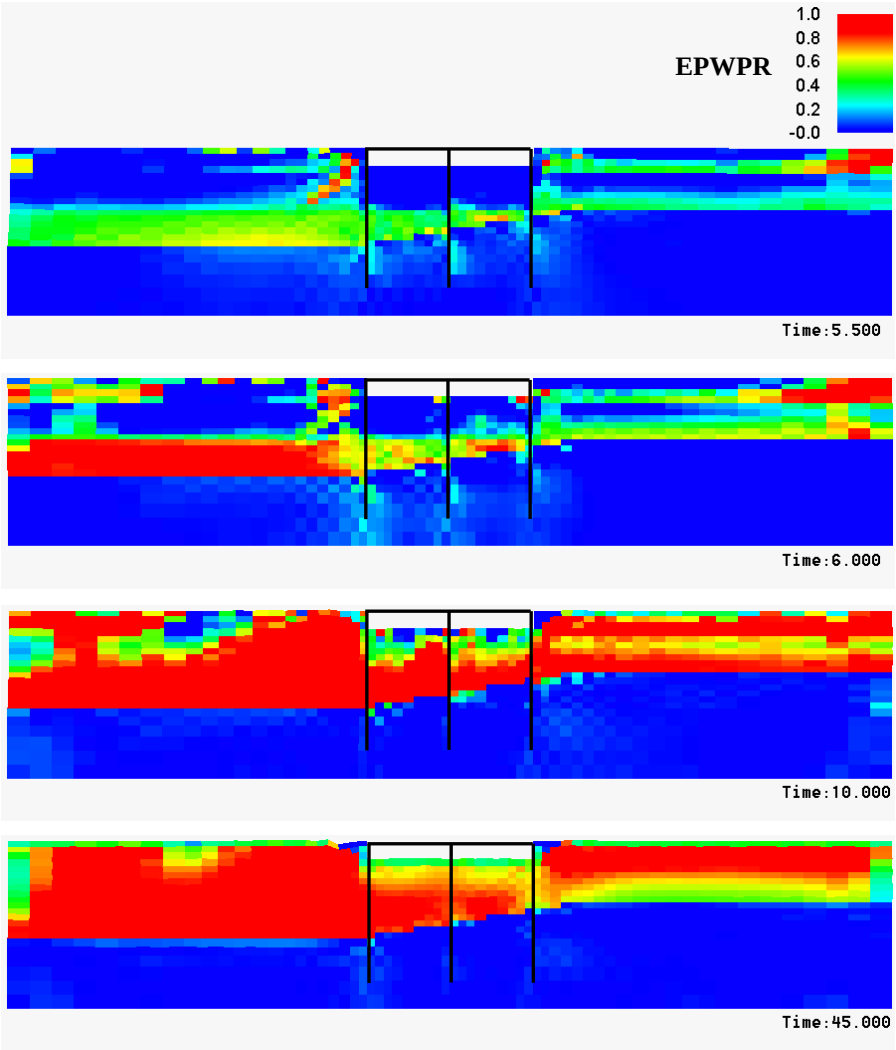

Figure 4: Development of excess pore water pressures and eventual liquefaction in the model during the deterministic analysis.

Figure 5 illustrates the acceleration and displacement histories at various depths 45 m to the left of the bridge (i.e. in the 'free-field', where there is negligible interaction with the bridge structure). It can be seen that in the N_1 = 30 layer (depths greater than 17.5 m) there is amplification of the acceleration response and negligible changes in the frequency characteristics of the motion. The effect of liquefaction in the bottom N_1 = 10 layer (11 m-17.5m) can be seen in the reduction of the peak acceleration to 0.299g at 12.1 m and also a significant peak displacement of 0.139 m at the same depth. The effect of liquefaction is also prevalent in the change in the frequency content of

acceleration histories in the upper 10 m after 7.0 s.

Figure 6a illustrates excess pore water pressure ratios 45 m to the left of the bridge. The three depths of z = 6.15, 14.75, and 19.75 m are located in the N_1 = 15, 10, and 30 layers, respectively. In accordance with Figure 4, it can be seen that complete liquefaction of the N_1 = 10 (i.e. z = -14.75m) layer by 7.0 s causes the removal of high frequency waves in the upper 10 m of the model. The liquefaction of the bottom N_1 = 10 layer also reduces the ground motion intensity in the above soil layers, which prevents full liquefaction from eventuating at z = 6.15m. Figure 6b illustrates the shear stress-strain response of the soil at z = -14.75m. It can be seen that following dilation to a shear stress of ~63 kPa, the soil liquefies and the response is characterised by very low shear stiffness and shear strains up to 2.5%.

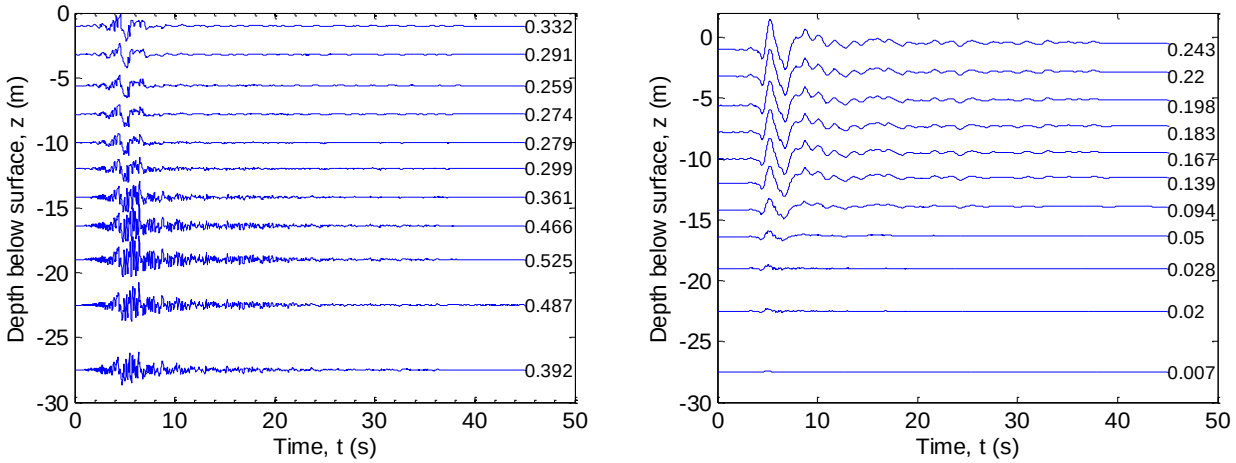

Figure 5: Response histories in the north free-field (x=20 m in Figure 2): (a) acceleration; and (b) displacement. Peak values are given at the end of each response history.

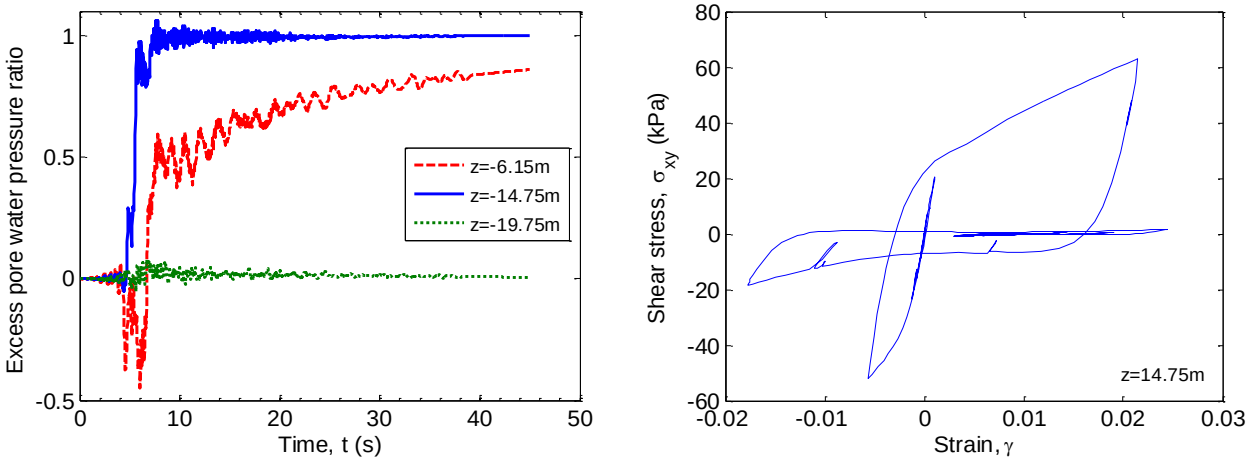

Figure 6: (a) Typical excess pore water pressure ratio development in the north free field (x=20 m in Figure 2); and (b) shear stress-strain response.

5.1.2 *Bridge and pile response*

Figure 7a illustrates the displacement time histories at the three footings of the bridge, and the north and south free-field response (all at a depth of z = -3.2 m). In the first 7.0 s, it is apparent that the displacement in the north free-field is larger than the south free-field and footing displacements, which are essentially identical. After 7.0 s relative displacements between the three footings becomes apparent due to significant liquefaction occurring in the surrounding soils. It is also apparent in Figure 7a that the displacement histories of the footings appear not completely in-phase with the free-field responses (both north and south). Figure 7b provides a comparison of the acceleration histories at the

north free-field (z = 0 m), central pile cap, and at 27.5 m depth, near the base of the model. It can be seen that the stiffening effect of the pile foundations allows waves of significantly higher amplitude and frequency to propagate to the central pier cap than to the free-filed surface, thus the reason for the aforementioned out-of-phasing and smaller amplitude of the footing displacements in Figure 7a compared to that in the free-field.

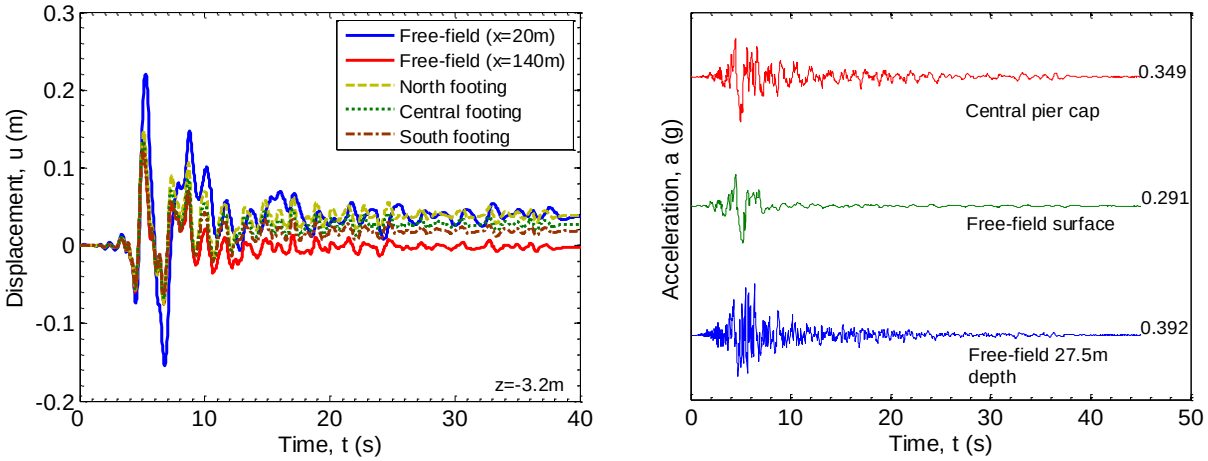

Figure 7: (a) displacement response history of the free field and at the pile footings; and (b) comparison of input, free-field, and pier cap acceleration histories.

Figure 8a illustrates the bending moment profiles in piles and abutments/pier at $t = 5.15$ s which corresponds to the peak footing displacements in Figure 7a. It can be seen that the seismic demand on the pile foundations is significant with both north and central piles exceeding their respective yield moments, and the south pile exceeding the cracking moment. The variation in the $N_1 = 10$ - $N_1 = 30$ boundary depth (e.g. Figure 2) is also observed to have a pronounced effect on the depth at which the peak negative bending moment is developed in the piles. The effect of this depth variation also causes larger soil displacements on the north side of the model relative to the south. As the large axial stiffness of the bridge superstructure effectively enforces equal displacements of the top of the abutments (with the exception of seating displacement discussed in the next paragraph), this variation in soil displacements in the horizontal direction also causes significantly different moments in the upper half of the piles and the abutments/pier. Figure 8b illustrates the shear force histories for the two abutments and central pier. It is immediately evident that forces in the north and south abutments are of opposite sign indicating that the bridge superstructure is predominately restraining the displacements of the north abutment/pile (where soil displacements are relatively large), and increasing the displacement of the south abutment/pile (where soil displacements are relatively smaller).

Figure 9 illustrates the relative displacement between the bridge superstructure and abutment (herein referred to as seating displacement) at the north and south abutments (the superstructure is fixed to the central pier). While for this particular ground motion the absolute value of the seating displacements are small (~1cm) compared with those necessary to cause unseating failure, this effect may be more important for higher levels of ground motion. In addition, correctly modelling the seating displacement also restricts the maximum shear force which can be transmitted between the bridge superstructure and abutments, which was observed to reduce the bending moments in the north and south abutments relative to those in the central pier.

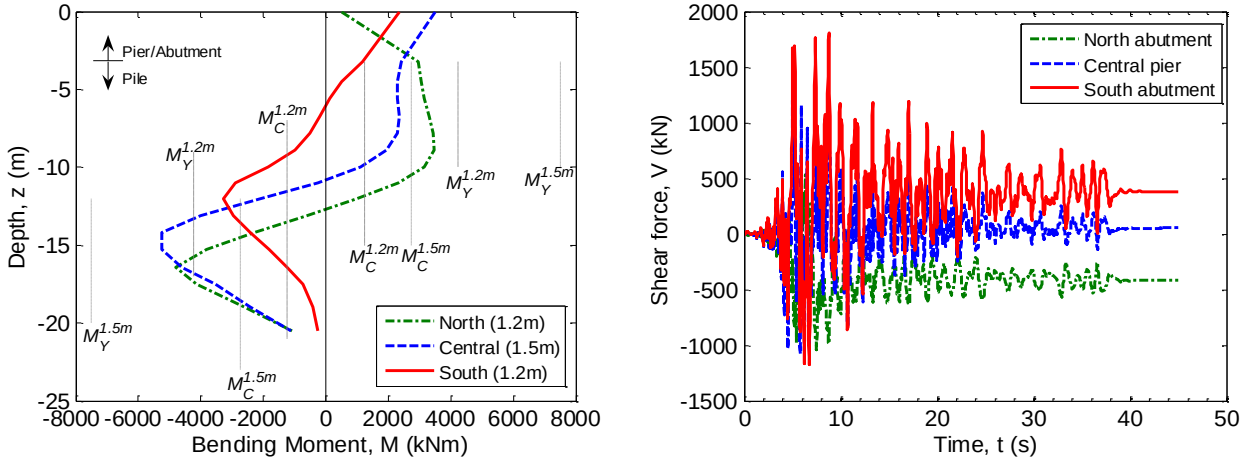

Figure 8: (a) bending moment profiles of the pile foundations at t=5.15s; and (b) shear force time histories in the abutments/pier.

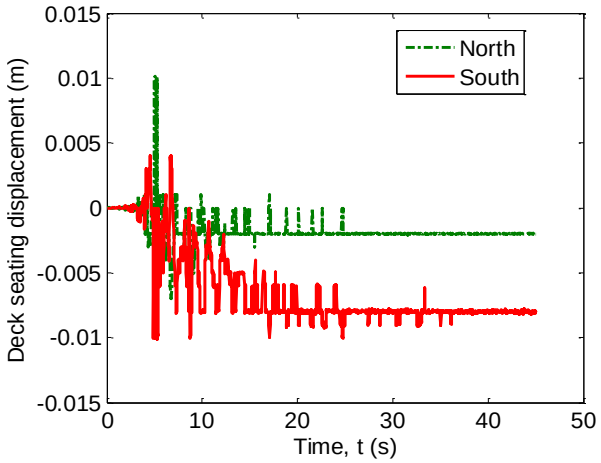

Figure 9: Deck seating displacement at the north and south abutments.

6 PROBABILISTIC SEISMIC RESPONSE AND SEISMIC DEMAND HAZARD

6.1 *Probabilistic seismic response analyses*

Clearly a vast amount of information and insight into the seismic response of the entire bridge-pile-soil foundation is possible by rigorously examining such seismic effective stress analyses discussed in the previous section. Based on the observations of various deterministic analyses, a total of nine different engineering demand parameters (EDP's) were monitored in each of the probabilistic seismic response analyses discussed in this section. These EDP's were: the peak curvature throughout the length of each of the three piles; the peak curvature in the abutments and central pier; the maximum seating displacement at the two abutments; and the maximum value of the settlement of the gravel approaches to the bridge superstructure. Due to space limitations only the EDP|IM plot for a single EDP is discussed below.

Figure 10 illustrates the results of the seismic response analyses for twenty ground motions at nine intensity levels for peak curvature in the north pile. Several points are worthy of note in Figure 10. Firstly, as expected the demand increases with an increase in the input ground motion intensity. Secondly, there is a large amount of dispersion in the results (e.g. for *PGA* = 0.46 g the peak curvature in the north pile ranges from 0.0004-0.005). This large dispersion occurs because of the acknowledged inefficiency of *PGA* as a ground motion intensity measure for the seismic response of

soft soil deposits.

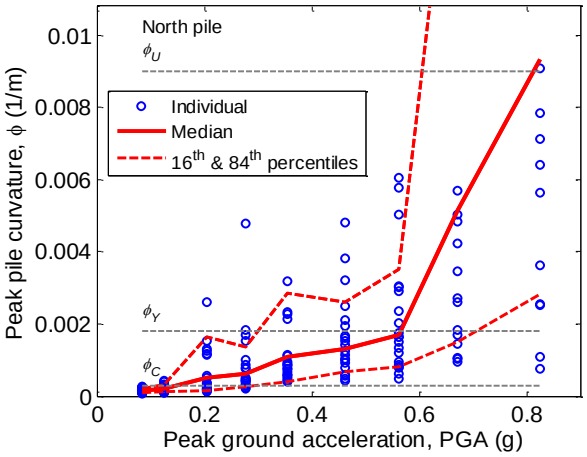

Figure 10: Example probabilistic seismic response analysis results for the north pile foundation.

6.2 *Seismic demand hazard*

By combining the seismic response analyses obtained in the previous section, which account for the variability in response due to the complexity of the ground motion excitation, with the seismic hazard curve in Figure 3a it is possible to compute the demand hazard curve for each of the different EDP's monitored. The demand hazard curve gives the annual frequency of exceeding a specified level of demand. Mathematical details can be found in Bradley et al. (2008).

Figure 11a illustrates the demand hazard curves for peak pile curvature for each of the three piles in the computational model. The effect of the variation in demand for the piles observed in Figure 10 is also apparent in the demand hazard curves. Based on the monotonic moment-curvature relationship of the piles, cracking, yielding, and ultimate damage states are also given in Figure 11a. It can be seen that the north and south piles are more vulnerable (i.e. have higher damage state exceedance frequencies) than the larger central pile, with the north pile significantly more vulnerable than the south pile, for higher levels of curvature. Figure 11b illustrates the demand hazard curves for the peak curvature of the abutments and central pier. As observed in Figure 10, it can be seen that the demand on the central pier is significantly greater than the north and south abutments, with the central pier having annual damage state exceedance frequencies typically an order of magnitude larger than the abutments.

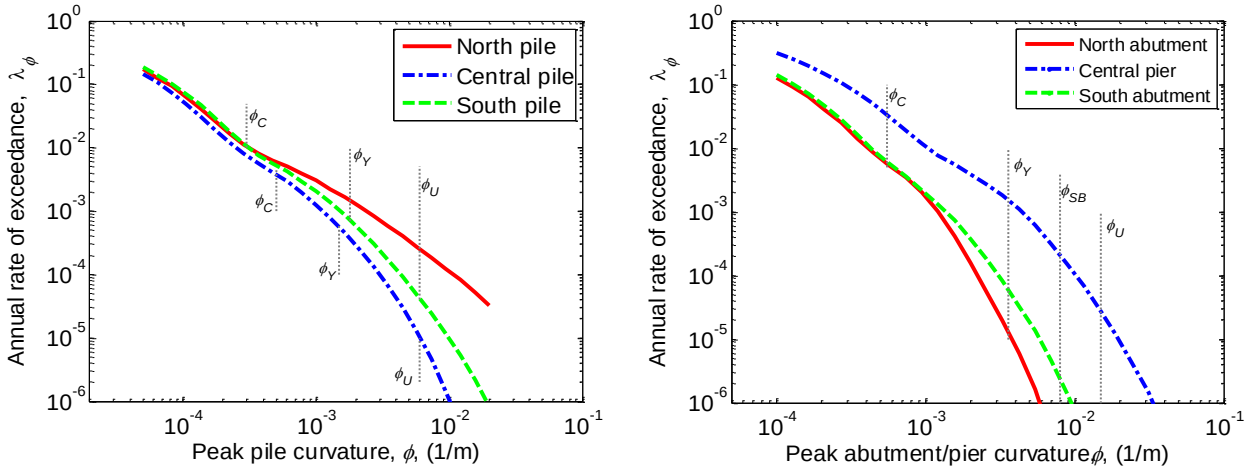

Figure 11: demand hazard curves for: (a) peak pile curvature; and (b) peak abutment/pier curvature.

Although not shown here, demand hazard curves for seating displacement and maximum approach settlements were also computed, but were found not to be critical in the seismic performance of the bridge-foundation-soil system. Using relationships between demand, damage and loss for the nine demand measures used here it is possible to create loss hazard curves (loss vs. annual frequency of exceedance). Such loss hazard curves allow coupling of the likelihood of demand occurrence with the consequences of its occurrence, and are useful in communicating seismic risk to non-engineering stakeholders (Bradley, et al. 2008).

7 CONCLUSIONS

This paper has presented the probabilistic seismic performance assessment of an actual bridge-foundation-soil system, the Fitzgerald Avenue twin bridges. The significant insight which can be gained regarding bridge-foundation-soil interaction and associated non-linearities using effective stress analysis was illustrated for a particular ground motion. The significant uncertainty regarding the input ground motion was addressed by subjecting the model to twenty different ground motions at nine different intensity levels to obtain probabilistic relationships between various engineering demand parameters (EDP's) and the ground motion intensity measure (IM), which was peak ground acceleration, *PGA*. By combining the probabilistic EDP|IM relationships with the ground motion hazard curve, it is possible to compute the demand hazard for the various EDP's and compare them to various damage states for each of the components.

It was observed that the non-horizontal soil profile layering and soil liquefaction were key factors in the response of the bridge-foundation-soil system. The critical components governing the seismic performance of the system were the north abutment piles and the central pier, which had the highest annual frequencies of exceeding various damage states.

8 ACKNOWLEDGEMENTS

Financial support from the New Zealand Tertiary Education Commission and the New Zealand Earthquake Commission is greatly appreciated.

REFERENCES:

Bradley B.A. Dhakal R.P. Cubrinovski M. MacRae G.A. Lee D.S. 2008.Seismic loss estimation for efficient decision making. *Bulletin of the New Zealand Society for Earthquake Engineering*.

Diana-J3 1987. Finite-element program for effective stress analysis of two-phase soil medium. Taisei Corporation internal report 1997 [in Japanese] ed: Software science.

Bowen H. Cubrinovski M. 2008.Effective stress analysis of piles in liquefiable soil: A case study of a bridge foundation. *Bulletin of the New Zealand Society for Earthquake Engineering,* 41 (4). 247-262.

Cubrinovski M. Bradley B.A. 2009 Evaluation of seismic performance of geotechnical structures.in *International Conference on Performance-Based Design in Earthquake Geotechnical Engineering — from case history to practice*, Tokyo, Japan, 16pp.

Cubrinovski M. Ishihara K. 1998.Modelling of Sand Behaviour based on state concept. *Soils and Foundations,* 28 (3). 115-127.

Bradley B.A. Cubrinovski M. Dhakal R.P. MacRae G.A. 2008.Intensity measures for the seismic response of pile foundations. *Soil Dynamics and Earthquake Engineering*.

Shome N. Cornell C.A. 1999. Probabilistic seismic demand analysis of nonlinear structures. Stanford University, Stanford, CA, Report No. RMS-35, RMS Program, 357pp.

Stirling M.W. Gerstenberger M. Litchfield N. McVerry G.H. Smith W.D. Pettinga J.R. Barnes P. 2007. Updated probabilistic seismic hazard assessment for the Canterbury region. 58pp.